Archives of Civil and Mechanical Engineering (2020) 20:44
https://doi.org/10.1007/s43452-020-00049-7

ORIGINAL ARTICLE

Experimental study on seismic performance of double-level yielding buckling-restrained braced concrete frames

Zhe Zhang[1] · Sheng-Nan Zhang[1] · En-Feng Deng[1] · Tong-Tong Zhou[1] · Yu Yi[2] · Hao He[2] · Na-Na Li[2]

Received: 12 December 2019 / Revised: 20 March 2020 / Accepted: 26 March 2020 / Published online: 4 April 2020

Abstract

This paper focused on the seismic performance of buckling-restrained braced concrete frame. Two different systems including the single-level yielding buckling-restrained braced concrete frame (SYBRBCF) and the double-level yielding buckling-restrained braced concrete frame (DYBRBCF) were designed for comparison. Compared with the single-level yielding buckling-restrained braces which are similar to many existing types of buckling-restrained braces, the double-level yielding buckling-restrained braces (DYBRBs) have two different energy absorption mechanisms that are expected to provide energy dissipations under the frequent earthquakes and rare earthquakes. To comparatively investigate the seismic performances of the two systems, cyclic tests were performed on one DYBRBCF specimen and another SYBRBCF specimen. The seismic response including the hysteretic curves, backbone curves, ductility coefficients, equivalent damping ratios, strengths, and stiffness degradations of the two experimental specimens was compared and analyzed. The test results indicate that the properly designed SYBRBCF and DYBRBCF can both exhibit the full hysteretic curves, meet the strong-column–weak-beam design requirement, and achieve the expected seismic performance. However, it was found that the ductility coefficient and energy dissipation capacity of the DYBRBCF were 72.2% and 23.4% higher than those of the SYBRBCF. The present study also provided useful design recommendations, which were beneficial to promote the application of DYBRBs.

Keywords Buckling-restrained braces · Double-level yielding · Single-level yielding · Concrete frame · Seismic performance · Cyclic test

1 Introduction

Reinforced concrete frames are widely used in many structural applications. However, when the frames do not meet the seismic requirements, dampers, and braces are generally necessary to improve their seismic performance. Ranaei et al. [1] and Massumi et al. [2] investigated the seismic performance of a new damper and bracing system, respectively. Dampers are useful in providing additional damping under frequent earthquakes. Braces are useful for the lateral stiffness under rare earthquake events. However, the lateral load-carrying capacity of the frames decreases rapidly after the yielding of the braces. Furthermore, the unbalanced capacity under tension and compression of the braces results in a poor energy consumption. Accordingly, buckling-restrained braces (BRBs) are important in improving the seismic performance of a structure. BRBs consist of the core material and an external restraining system, which generally include steel tubes and a concrete filler (Fig. 1). The core material can yield under tension and compression and dissipate seismic energy. The restraining system

✉ En-Feng Deng
dengenfeng@zzu.edu.cn

Zhe Zhang
zhangzhe_77@163.com

Sheng-Nan Zhang
594986369@qq.com

Tong-Tong Zhou
791768527@qq.com

Yu Yi
403703090@qq.com

Hao He
6973858@qq.com

Na-Na Li
463358202@qq.com

1 School of Civil Engineering, Zhengzhou University, Zhengzhou 450000, China

2 Henan Urban Planning Institute and Corporation, Zhengzhou 450000, China

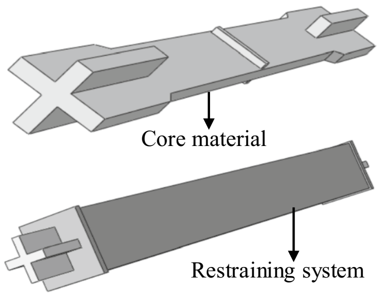

Fig. 1 Configuration of the BRB

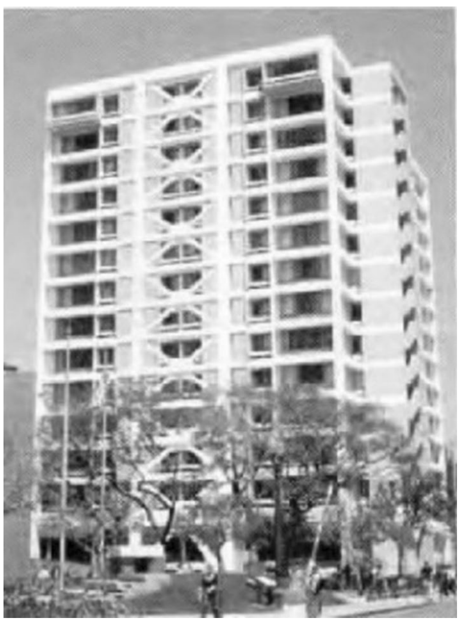

Fig. 2 Example of BRBs in concrete frame [4]

not only restrains the lateral deformation; it also increases the lateral stiffness of the structure [3]. BRBs have been widely used in concrete structures to improve their seismic behavior, as shown in Fig. 2 [4]. The study of BRBs originated in Japan during the late 1980s [5]. In 1989, BRBs were applied in buildings [6]. Many scholars have conducted considerable research during the past decades in this area. Various types of BRBs have been tested. Bozkurt et al. [7] proposed the use of welded overlap core encased BRBs. Zhu et al. [8] introduced corrugated-web connected BRBs. Qu et al. [9] studied buckling-restrained brace (BRB) with replaceable steel angle joint. In addition, Guo et al. [10, 11] presented several core-separated buckling-restrained braces and conducted the elastic buckling analysis. They also proposed an innovative core-separated battened buckling-restrained brace [12]. The experiment results showed that the BRBs exhibit a good seismic performance. Wang et al. [13] designed and tested BRBs with various gusset connections under axial cyclic loading to ensure a reliable connection. Tsai et al. [14] proposed a performance-based design method of the gusset connections incorporating a BRB and frame. It has been demonstrated that K-brace [15], double-K-brace [16], and O-brace [17] can be considered in practice. BRBs are also effective reinforcements for an insufficient seismic performance of the existing structures [3]. Several researchers have adopted a finite element analysis (FEA) to understand the mechanical behavior of buckling-restrained braced concrete frames (BRBCFs). Chou et al. [18] presented the FEA of a sandwiched all-steel assembled BRB. An evaluation method was also developed for the FEA to compute the rotational stiffness and strength of the gusset plate [19]. In addition, AlHamaydeh et al. [20] used a nonlinear FEA to study the key influencing parameters and failure modes of BRBs.

However, BRBs show a good energy consumption only under rare earthquake events. Li et al. [21] proposed a new type of double-level yielding buckling-restrained braces (DYBRBs) as a combination of conventional BRBs and metal dampers to improve the energy dissipation capacity of structures under frequent earthquake events. Two DYBRBs with different configurations of tube dampers were tested to investigate their low-cycle fatigue resistance under frequent earthquakes and seismic performance. It was reported that the hysteresis curves of DYBRB specimens were stable and full. The low-cycle fatigue resistance of DYBRBs was demonstrated to be excellent. Sun et al. [22] conducted the parametric analysis of frames with DYBRB under frequent earthquake. Furthermore, the corresponding design suggestions were proposed. However, the previous research merely focused on the seismic performance of the DYBRB. The seismic performance of the moment frame braced by DYBRB remains unknown.

In this study, a single-level yielding buckling-restrained braced concrete frame (SYBRBCF) and a double-level yielding buckling-restrained braced concrete frame (DYBRBCF) were tested. Cyclic loading test was conducted to assess the seismic performance of the concrete frames with single-level yielding buckling-restrained braces (SYBRBs) and double-level yielding buckling-restrained braces (DYBRBs). Initially, the working mechanism of the DYBRBs was introduced. The test results were then discussed and compared in terms of the hysteretic curves, skeleton curves, ductility, strength degradation, stiffness degradation, and energy dissipation capacity. This paper presents good evidence of the good seismic performance of DYBRBs, which may provide useful guidance for the engineering practice of such braces.

2 Mechanism of DYBRBs

DYBRBs consist of conventional BRBs and metal tube dampers. Figure 3 shows the configuration of the DYBRBs. The BRBs are connected with the metal tube dampers with

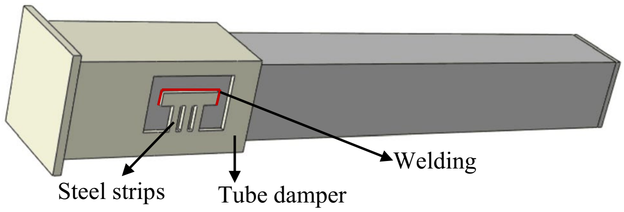

Fig. 3 Configuration of the DYBRB

a small gap to ensure their convenience, with the other end free. The free ends of the steel strips of the metal tube dampers are connected with the BRBs through fillet welding. The damping of the system is based on the yield of the steel strips when the load reaches the yielding load. The yielding load of the steel strips is considerably smaller than that of the core material. With an increase in the relative displacement of the two ends of the BRBs, the steel damper yields first. The core material then yields, achieving a double-level yielding mechanism. The working stage of the DYBRBs can be divided into four stages based on the configuration. During the elastic stage, neither the core material nor the tube damper achieves the yielding load. During the first-level yielding stage, the core material remains elastic, with the steel strips of the tube damper yielding. Within the double-level yielding stage, the core material and the tube damper yield. Finally, during the failure stage, the tube damper is destroyed and only the core material dissipates energy. The diagrammatic sketch of the relationship between axial force (P) and axial stiffness (Δ) in the whole working stage is shown in Fig. 4.

To understand the mechanism of the DYBRBs, the relationship between the axial force (P) and the axial displacement (Δ), as well as the stiffness formulas, is presented as follows [21]:

During the elastic stage ($\Delta \leq (1+\frac{k_D}{k_T})\Delta_{Dy}$),

$$P_1=\left(\frac{1}{\frac{1}{k_D+k_T}}+k_C\right)\Delta, \quad (1)$$

$$k_1=\frac{1}{\frac{1}{k_D+k_T}}+k_C. \quad (2)$$

During the first-level yielding stage ($(1+\frac{k_D}{k_T})\Delta_{Dy} \leq \Delta \leq \Delta_{Cy}$),

$$P_2=\left(\frac{1}{\frac{1}{\beta_D k_D}+\frac{1}{k_T}}+k_C\right)\Delta+\frac{\frac{1}{\beta_D}-1}{\frac{1}{\beta_D k_D}+\frac{1}{k_T}}\Delta_{Dy}, \quad (3)$$

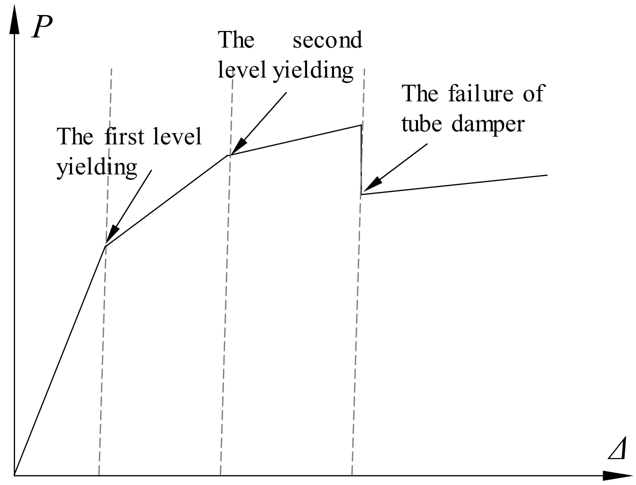

Fig. 4 Skeleton curve of the DYBRB

$$k_2=\frac{1}{\frac{1}{\beta_D k_D}+\frac{1}{k_T}}+k_C. \quad (4)$$

During the double-level yielding stage ($\Delta \geq \Delta_{Cy}$),

$$P_3=\left(\frac{1}{\frac{1}{\beta_D k_D}+\frac{1}{k_T}}+\beta_C k_C\right)\Delta+\frac{\frac{1}{\beta_D}-1}{\frac{1}{\beta_D k_D}+\frac{1}{k_T}}\Delta_{Dy}+\left(1-\beta_C\right)k_C\Delta_{Cy}, \quad (5)$$

$$k_3=\frac{1}{\frac{1}{\beta_D k_D}+\frac{1}{k_T}}+\beta_C k_C. \quad (6)$$

During the failure stage ($k_D=0$, $P_D=0$),

$$P_4=\beta_C k_C\Delta+\left(1-\beta_C\right)k_C\Delta_{Cy}, \quad (7)$$

$$k_4=\beta_C k_C, \quad (8)$$

where k_C, k_T, and k_D are the stiffness parameters of the core material, tube damper, and restraining system, respectively; Δ_{Cy} and Δ_{Dy} are the yielding displacements of the core material and tube damper, respectively; and β_C and β_D are the reduction coefficients of the core material and the post-yielding stiffness of the tube damper, respectively.

3 Experimental program

3.1 Test specimens

Cyclic tests of two one-story one-bay concrete frames were conducted. One frame was upheld using a SYBRB, and the other was upheld using a DYBRB. The specimens based on a school building in Xinxiang, China were designed in accordance with the Chinese code for the seismic design of buildings (GB50011-2010(2016)) [23] and the design of concrete structures (GB50010-2010(2015)) [24]. The span length (center to center) and story height of the specimens were 2520 mm and 2260 mm, respectively. The key parameter of the specimens was the type of BRB applied. Therefore, the concrete grade, reinforcement grade, reinforcement ratio, and dimensions of the gusset plate were identical.

3.1.1 Details of the concrete frame

The longitudinal rebars and stirrups were of an HRB400 reinforcement. The flexural strength of beam and column is adjusted accordingly based on Chinese seismic design code (GB50011-2010(2016)) [23] to achieve the strong-column–weak-beam concept. Figure 5 shows the sections of the components and the geometric dimensions of the frames. Each test specimen consisted of 3370 mm high (overall dimension), 240 mm × 240 mm columns, and 3160 mm long (overall dimension), 140 mm × 240 mm beams. The measured cube strengths of concrete of the columns and beams were 49 MPa and 47 MPa, respectively. The concrete frames were cast using an embedded part with 12 M16 studs (16 mm in diameter). The gusset plates were then welded to the embedded part. The frames and BRBs were connected by gusset plates at the beam–column joints. A reduced stirrup spacing was adopted to strengthen the local cross sections of the joint areas in accordance with the Chinese seismic design code (GB50011-2010(2016)) [23].

3.1.2 Details of the BRBs

The SYBRBs and DYBRBs were designed and manufactured as shown in Fig. 6 and Table 1. The design of BRBs is mainly based on the stiffness and yield displacement to meet the specified story drift ratio. The restraining system of the BRBs consisted of a 150 mm × 150 mm × 12 mm hollow steel section and C30 concrete filler. The Q235B grade steel (nominal yielding stress of 235 MPa) was used for the core material and restraining steel tube. As the design principles of the two BRBs, the yielding load of the SYBRBs and the second level yielding load of the DYBRBs were equal to 520 kN. The corresponding yielding load of DYBRBs and SYBRBs can be calculated by Eqs. (5) and (9) [25], respectively. The BRBs were transported to the laboratory after factory manufacturing. The BRBs were connected to the frames through site welding conducted in a laboratory.

$$P_y = f_y A_c \tag{9}$$

where P_y is the yielding load of the SYBRBs, f_y is the yielding stress of the core material, and A_c is the cross-area of the core material.

3.2 Test set-up and instrumentation

Figure 7 shows the details of the test set-up. Two specimens were tested in the structural laboratory of Zhengzhou University. A quasi-static testing procedure was used. The test was conducted using a servo-controlled hydraulic actuator with a force capacity of 2000 kN, the lateral force of which was recorded by a force transducer. The axial load of the columns of the two specimens was applied by the upper oil jacks and kept constant as 669 kN. This corresponds to 0.3 of the axial compression ratio based on the value range of Chinese seismic design code (GB50011-2010(2016)) [23]. The actuator and jacks were fixed to the reaction wall and frame, respectively. The loading cell consisted of steel plates at each end of the beams, and rods connected the specimens to the actuator. Two jacks arranged on each side of the bottom of the specimens acted together with the anchor bolts to restrict the horizontal movement of the specimens.

The displacement of the key points of the specimens was measured using a displacement transducer. Figure 8 shows the instrumentation of the test specimens. To measure the displacement of the upper beams of the specimens, two displacement meters ($D_{s,d}1$ and $D_{s,d}3$) were placed on each side of the upper beam. The functions of $D_{s,d}2$ and $D_{s,d}4$ are the same as those of $D_{s,d}1$ and $D_{s,d}3$, respectively. In addition, $D_{s,d}9$ and $D_{s,d}10$ were mounted to monitor the possible displacement of the lower beams of the specimens. A single-level yielding buckling-restrained braced axial deformation was obtained by $D_{s,d}6$ and D_s7 or $D_{s,d}5$ and D_s8, and a double-level yielding buckling-restrained braced axial deformation was obtained by D_d8. Moreover, D_d7 was used to measure the shear deformation of the steel strips of the mental damper, and $D_{s,d}11$ and $D_{s,d}12$ were placed to monitor the out-of-plane displacement of the specimens.

3.3 Loading protocol

The test was controlled through displacement during the test. Figure 9 shows a schematic of the loading program. Story drift ratios of 1/900, 1/500, 1/320, 1/220, 1/170, 1/130, 1/95, 1/75, and 1/50 were selected as the target amplitudes, and two cycles were imposed on the test specimens at each displacement amplitude. Finally, the last loading level was repeated until the failure of the specimens. DYBRBs can improve the energy dissipation capacity of structures under frequent earthquake events because of the mental damper. Additional displacement amplitudes of 1/2800, 1/2000, 1/1400, and 1/700 were added to DYBRBCF to better understand the energy dissipation capacity of the DYBRBCF under frequent earthquake events. In the test, the pull (from east to west, as shown in Fig. 7) and push (from west to east) were defined as the positive and negative loadings, respectively.

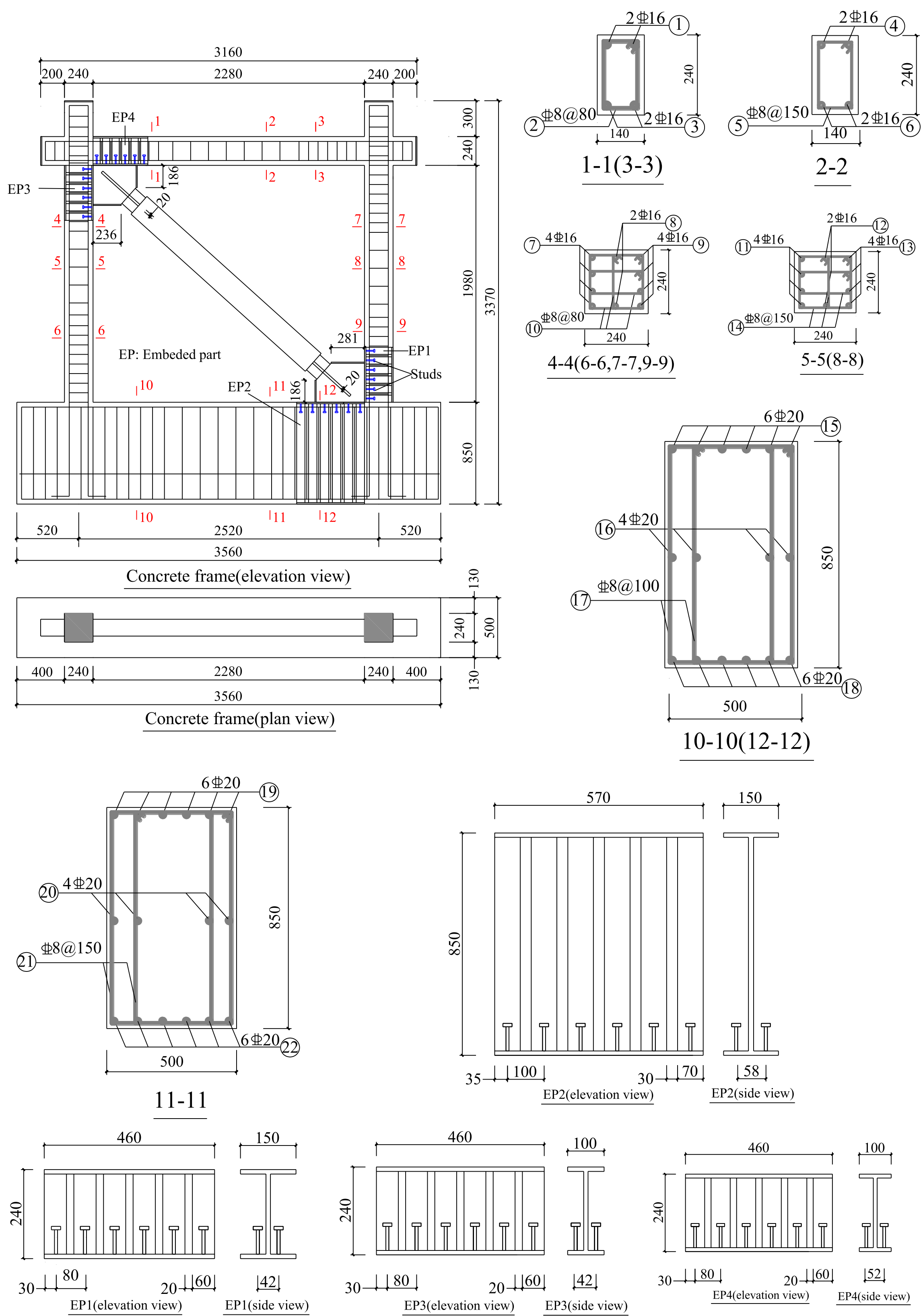

Fig. 5 Section and reinforcement of the concrete frame

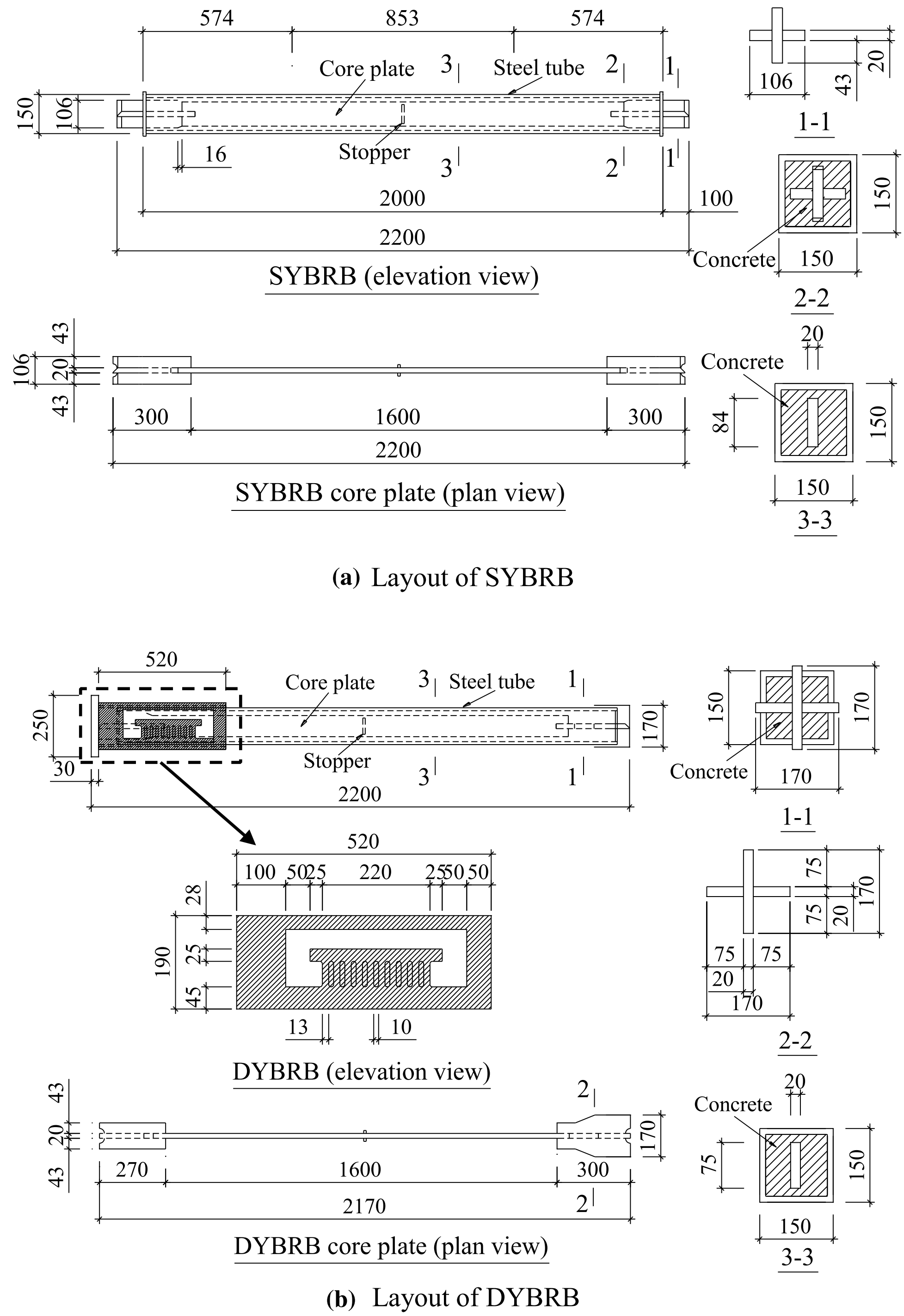

Fig. 6 Configuration of the BRBs

Table 1 Key parameters for the BRBs

Type of BRB	Angle (°)	Area of the core plate (mm^2)	Axial stiffness (kN mm^{-1})	Yield displacement (mm)	Yield load (kN)
SYBRB	41.9	1680	217	2.4	520
DYBRB	41.9	1500	First-level yielding: 267	First-level yielding: 0.6	First-level yielding: 160
			Second-level yielding: 217	Second-level yielding: 2.4	Second-level yielding: 520

Fig. 7 Test set-up. 1, actuator; 2, jack; 3, reaction wall; 4, reaction frame; 5, loading cell; 6, anchor bolt; 7, bottom beam; 8, rigid steel beam; 9, concrete frame; 10, BRB

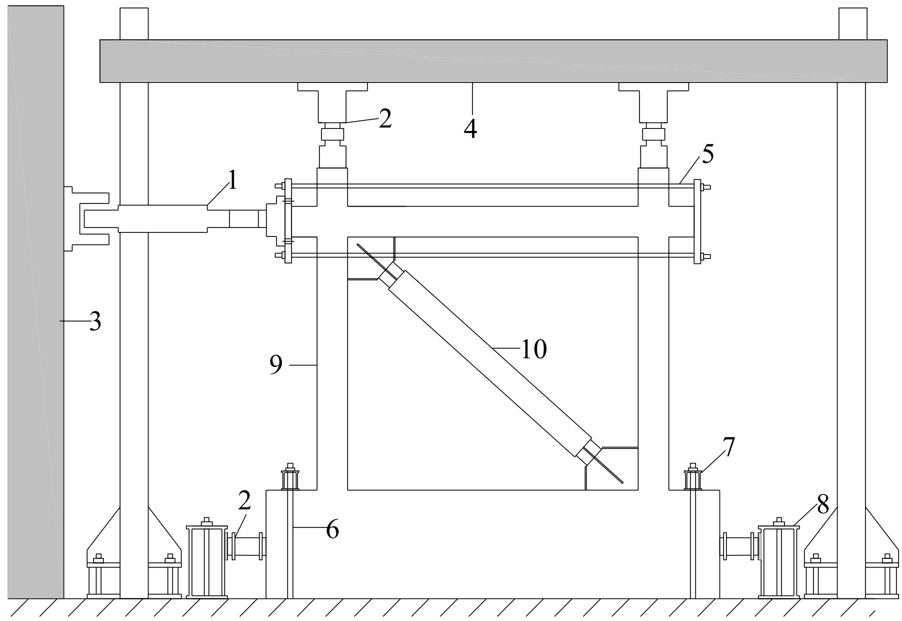

(a) Diagram of the test setup

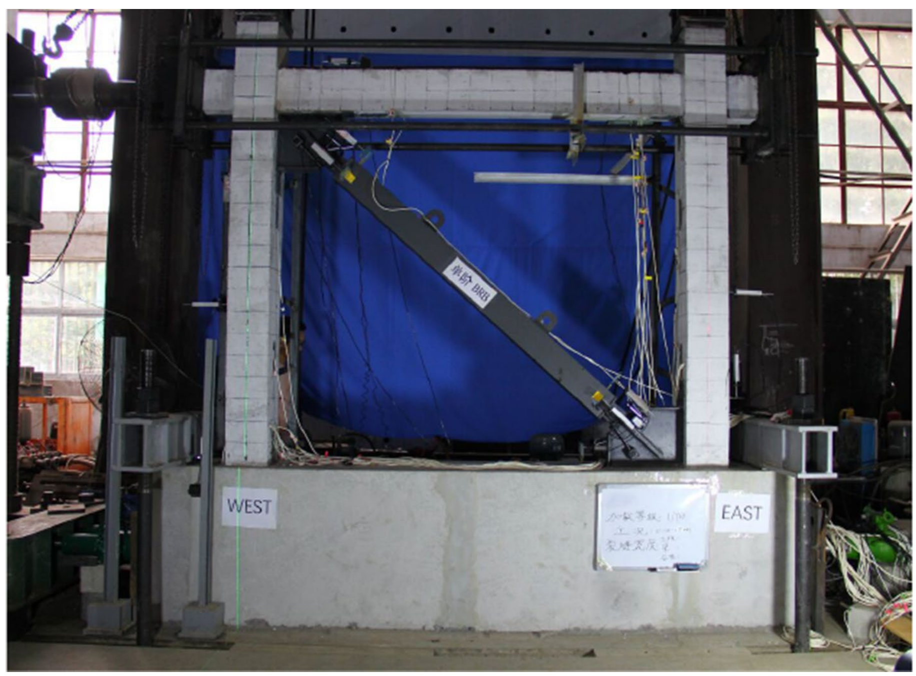

(b) Photograph of the test setup

4 Experiment observations

4.1 Failure process of SYBRBCF

Cracks at the beam appeared at the first cycle of the story drift ratio of 1/900, whereas minor cracks in the column were initially observed at the first cycle of story drift ratio of 1/500. At the second cycle of story drift ratio of 1/170, diagonal cracks at the bottom of the left column were detected, as shown in Fig. 10a. The cracks penetrated the middle of the right column at the first cycle of 1/95 story drift ratio. The width of the cracks increased gradually at the upper edge of the embedded parts of the right column.

With an increase in the displacement amplitude, concrete crushing occurred at the beams and columns. A deformation of the core material became evident, as shown in Fig. 10b. At a 1/75 story drift ratio, the widths of the crack at the right edge of the embedded part of the

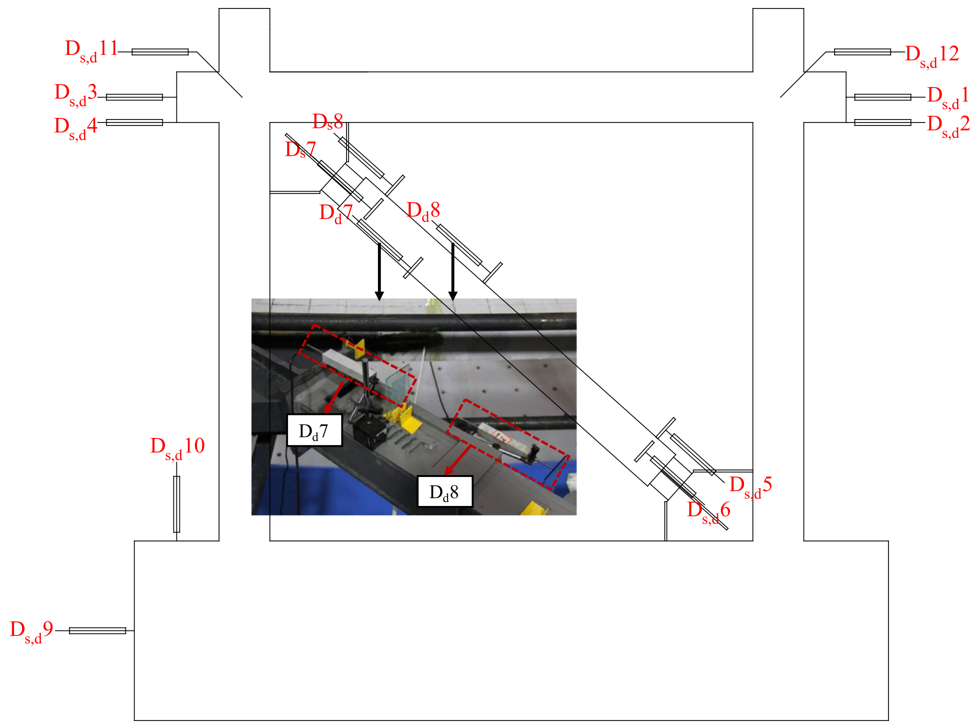

Fig. 8 Instrumentation of the test specimens

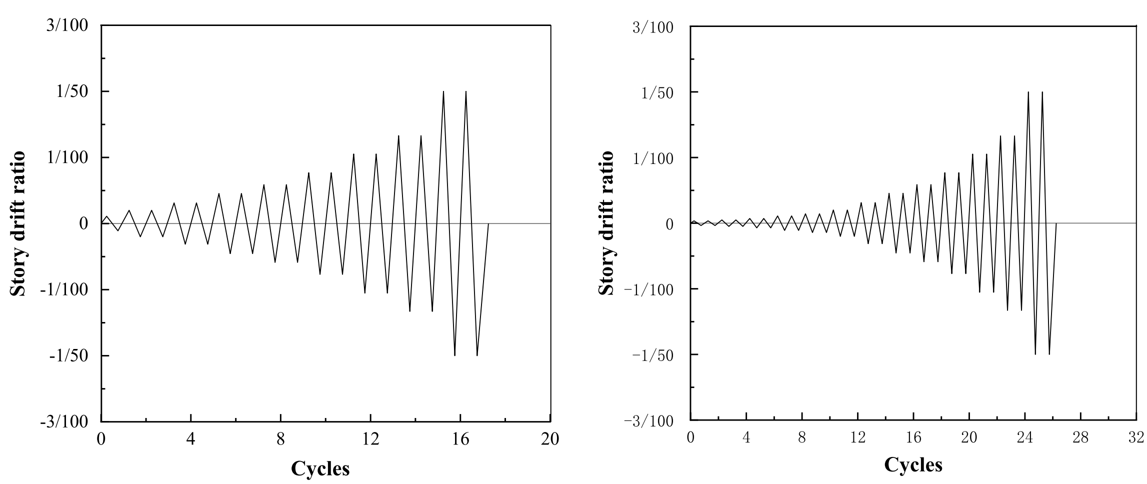

(a) SYBRBCF **(b)** DYBRBCF

Fig. 9 Loading program

beam and at the upper edge of the embedded part of the right column increased to 3.1 and 1.14 mm, respectively, accompanied by concrete crushing. The test was terminated owing to the evident plastic hinges of the beam at the second cycle of story drift ratio of 1/50 (as shown in Fig. 10c), accompanied by concrete crushing at the corner of the right column (as shown in Fig. 10d).

4.2 Failure process of DYBRBCF

Microcracks in the beams were initially observed at the second cycle of 1/700 story drift ratio, whereas those in the columns were initially observed at the first cycle of 1/500 story drift ratio. Cracks in the embedded part of the beams developed from bottom to top, and diagonal cracks

Fig. 10 Failure process of SYBRBCF

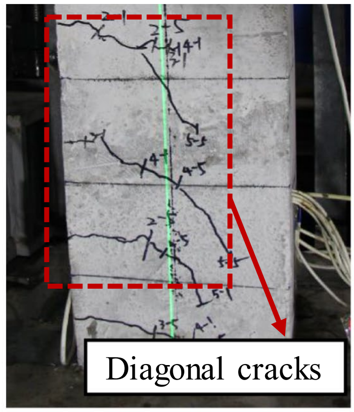

(a) Concrete cracks of the left column

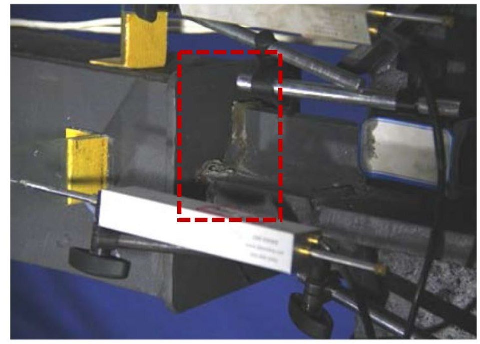

(b) Deformation of the core plate

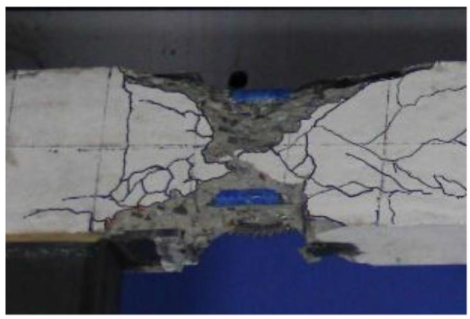

(c) Plastic hinge of the beam at the left column

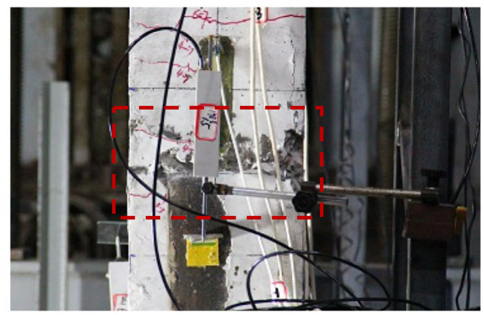

(d) Concrete cracks of right column

were initiated in the right column. The shear deformation of the steel damper was evident when the story drift ratio was 1/220, as shown in Fig. 11a. At the first cycle of story drift of 1/130, the steel damper was sheared off, as shown in Fig. 11b.

With an increase in the displacement amplitude, a slight crushing of concrete occurred at the right end of the beam, with a small amount of concrete peeling off. The width of the cracks in the left column reached 0.5 mm at a 1/75 story drift ratio. The concrete at the upper edge of the embedded parts of the right column was crushed, as shown in Fig. 11c. The test was terminated owing to the fast-growing plastic hinges at the right end of the beam at the third cycle of story drift ratio of 1/50, and concrete crushing was observed at the embedded part of the beams, as shown in Fig. 11d.

4.3 Comparisons and discussion

Overall, the concrete frames with SYBRB and DYBRB exhibited good ductility and energy consumption performance during the loading process. The BRBs and concrete frames work well with each other. The degree of damage to the beams, columns, and joints were relatively reduced at each loading level for the DYBRBCF as compared with the SYBRBCF. The damage was concentrated in the beam and column ends. The width and depth of the cracks of SYBRBCF were wider and deeper than those of DYBRBCF. The concrete of the two specimens was slightly crushed at the bottom of the left columns and seriously crushed in the embedded parts of the right column, as shown in Fig. 12. Plastic hinges occurred at the right joint and edge of embedded part of the beam of SYBRBCF, whereas a plastic hinge was only formed at the right joint of the beam of DYBRBCF, as shown in Fig. 13. This finding indicates that the two specimens satisfied the strong-column–weak-beam design concept. The ultimate load-bearing capacity of the DYBRBCF was 39.3% higher than that of the SYBRBCF.

5 Test results and analysis

5.1 Load–displacement hysteretic curves

Figure 14a–i shows the hysteretic curves of SYBRBCF and DYBRBCF at each loading level of SYBRBCF. Figure 14a–i indicates that the maximum value of the lateral force of the DYBRBCF was higher than that of the SYBRBCF at each loading level. Figure 14j compares the complete hysteretic curves of the specimens. In general, the hysteretic curves of the two specimens were full without evident pinching

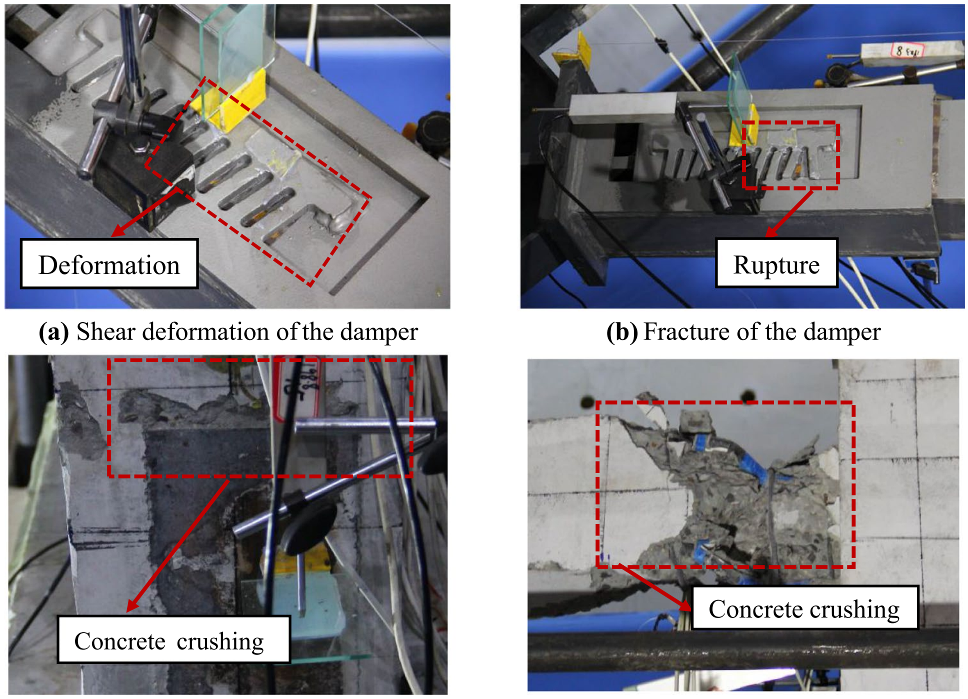

(a) Shear deformation of the damper **(b)** Fracture of the damper **(c)** Concrete crushing of the right column **(d)** Plastic hinge of the beam at the right column

Fig. 11 Failure process of DYBRBCF

phenomena. This result indicates that the SYBRBCF and DYBRBCF exhibited a good energy dissipation capacity. The load-bearing capacity of the specimens under lateral loads increased with an increase in the displacement amplitude.

The hysteretic curves of the DYBRBCF were fuller than those of the SYBRBCF, indicating a better energy dissipation capacity of the DYBRBCF. The horizontal force for each story drift ratio for the two specimens is shown in Table 2. The slight reduction in the DYBRBCF under the peak load at a 1/130 story drift ratio was due to the shear failure of the damper. The load-bearing capacity of the DYBRBCF continued to increase owing to the working of the core material. At the last loading levels, the trends of the hysteretic curves of the two specimens were similar. The reason for this observation was that the working mechanism of the DYBRBCF was the same as that of the SYBRB after the failure of the damper.

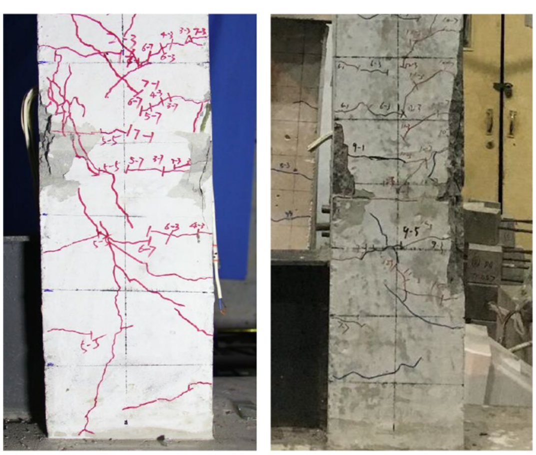

(a) SYBRBCF **(b)** DYBRBCF

Fig. 12 Concrete cracks of the column of the test specimens

5.2 Skeleton curves and ductility

The peak load in the positive and negative directions at each loading level was extracted to construct the skeleton curve, as shown in Fig. 15. During the test, the BRBs were sustained without failure. In general, no evident degeneration of the load-bearing capacity of the specimens occurred, except for a failure of the damper. When the concrete frames were destroyed at the last loading level, the lateral force of the two specimens reached their maximum value. The SYBRBCF and DYBRBCF exhibited a good load-bearing capacity.

The ductility can be evaluated by the ductility coefficient (μ), which is defined as the ratio of the ultimate displacement to the yield displacement, as given in Eq. (10). Table 3 lists the primary performance indicators of the test specimens. The yield story drift ratios of the DYBRBCF and SYBRBCF were 1/362 and 1/211, respectively, which indicates that the DYBRBCF initially proceeded into the plastic stage. However, the yield load of the DYBRBCF enhanced by 58.8%

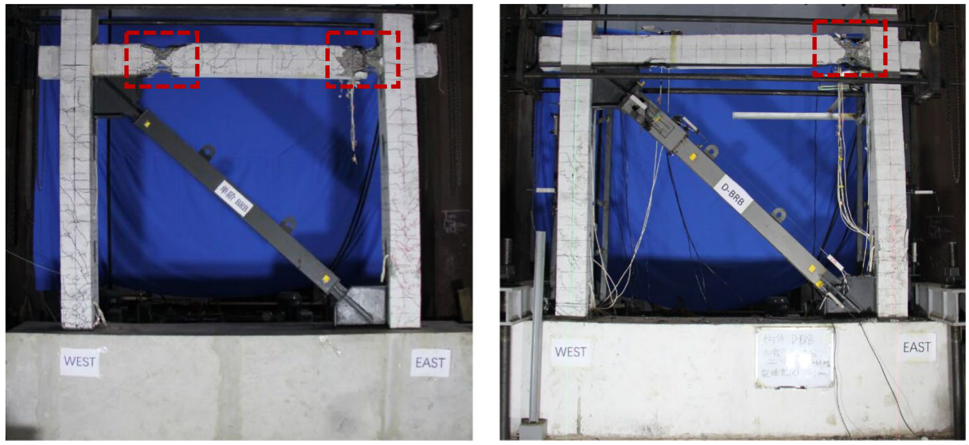

Fig. 13 Failure mode of the test specimens

(a) SYBRBCF **(b)** DYBRBCF

from 529 to 840 kN compared with that of the SYBRBCF. The ductility coefficients of the SYBRBCF and DYBRBCF were approximately 4.14 and 7.13, respectively, indicating that the two specimens exhibited a good ductility. The ductility can be used to evaluate the energy dissipation capacity of the specimens after yielding. The ductility coefficient of the DYBRBCF was 72.2% higher than that of the SYBRBCF, indicating the better deformation capacity of the DYBRBCF.

$$\mu = \frac{d_{\mathrm{u}}}{d_{\mathrm{y}}}, \tag{10}$$

where d_{u} and d_{y} are the ultimate and yield displacements, respectively.

5.3 Strength and stiffness degradation

A strength degradation is a decrease in the load-bearing capacity with an increase in the loading times at the same loading level. A strength degradation can be evaluated based on the strength degradation coefficient (λ_i), which is defined as the ratio of the peak load in the last cycle to the peak load in the first cycle at the same loading level, as given in Eq. (11) [26].

$$\lambda_i = \frac{P_j^i}{P_j^1}, \tag{11}$$

where P_j^i is the peak load of the last cycle at the jth loading level, and P_j^1 is the peak load of the first cycle at the jth loading level.

Figure 16 shows the strength degradation coefficients of the test specimens at different levels. A slight degradation in the strength of the DYBRBCF was detected owing to the failure of the damper. In general, the degradation in the strength of the SYBRBCF and DYBRBCF was slight in both the positive and negative directions during the entire loading process, indicating the stable load-bearing capacity of the specimens.

The scant stiffness (K_j), which is also known as the cyclic stiffness and is defined as the ratio of the cumulative peak load to the corresponding cumulative lateral displacement at the loading level of j, was utilized to evaluate the stiffness degradation of the specimens in this study, as given in Eq. (12) [26].

$$K_j = \frac{\sum_{i=1}^{n} P_j^i}{\sum_{i=1}^{n} u_j^i}, \tag{12}$$

where P_j^i is the peak load of the ith cycle at the jth loading level, u_j^i is the corresponding displacement of the ith cycle at the jth loading level, and n is the number of cycles at the corresponding loading level.

Figure 17 shows the scant stiffness of the specimens at different levels. During the entire loading process, the stiffness of the DYBRBCF was higher than that of the SYBRBCF. The failure stiffness was approximately 14.1–18.1% of the initial stiffness for the SYBRBCF, whereas it was approximately 9.0–11.1% of the initial stiffness for the DYBRBCF. The initial stiffness of the DYBRBCF was approximately 2.1 times that of the initial stiffness of the SYBRBCF attributed to the damper. The stiffness of the two specimens decreased continuously with an increase in the lateral displacement, and their stiffness degradation was steady and stable.

5.4 Energy dissipation capacity

The energy dissipation capacity is crucial for describing the seismic behavior of the specimens. The energy dissipation ratio E and equivalent damping ratio ξ_{e} can be accurately

Fig. 14 Hysteretic curves of the test specimens

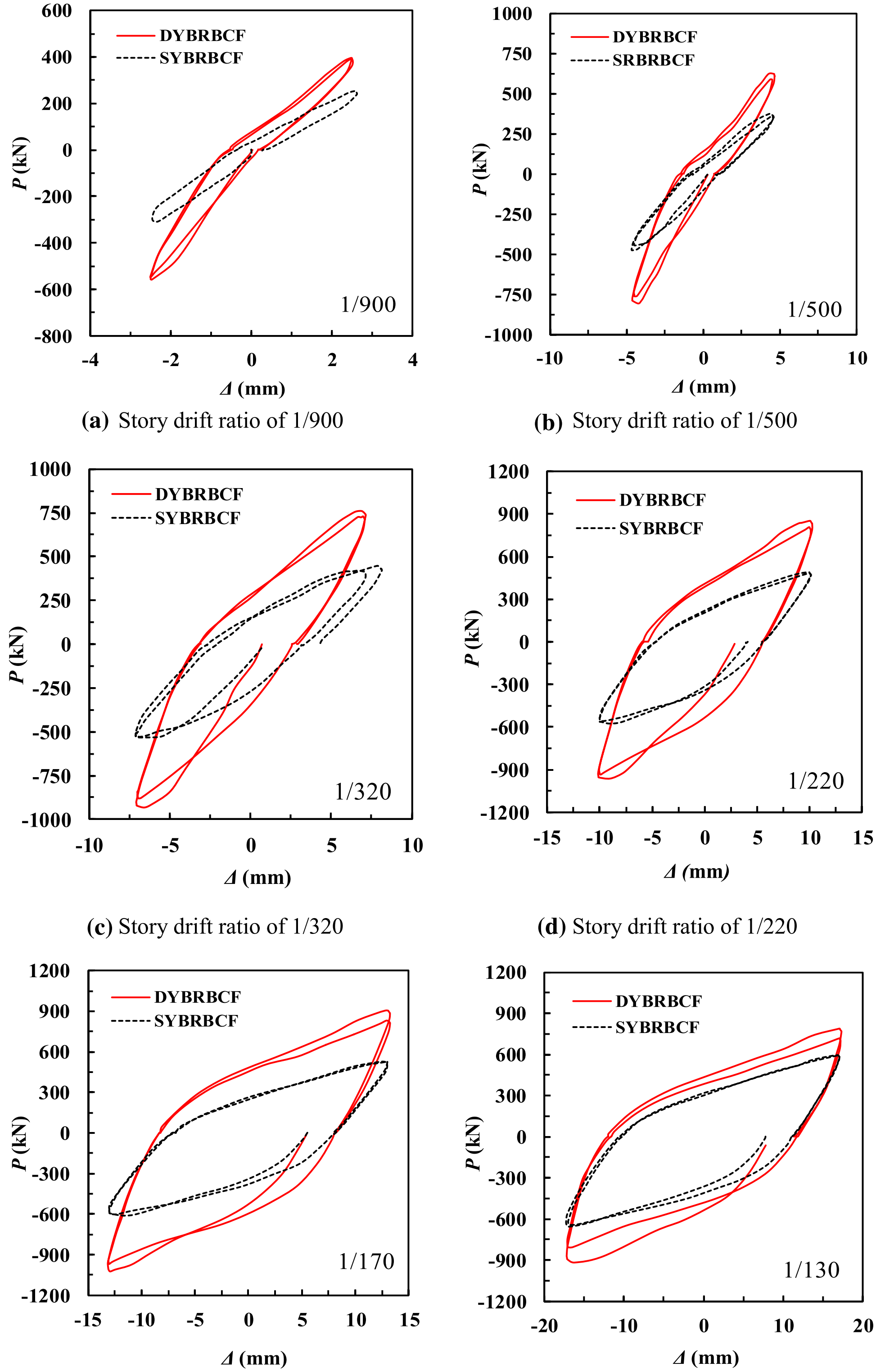

(a) Story drift ratio of 1/900

(b) Story drift ratio of 1/500

(c) Story drift ratio of 1/320

(d) Story drift ratio of 1/220

(e) Story drift ratio of 1/170

(f) Story drift ratio of 1/130

Fig. 14 (continued)

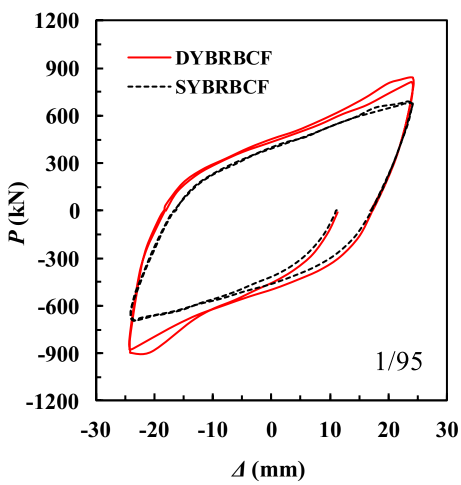

(g) Story drift ratio of 1/95

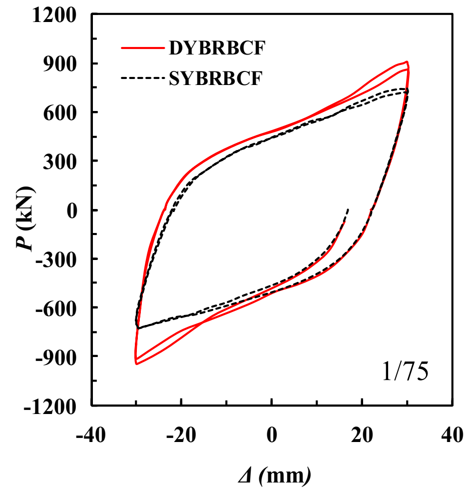

(h) Story drift ratio of 1/75

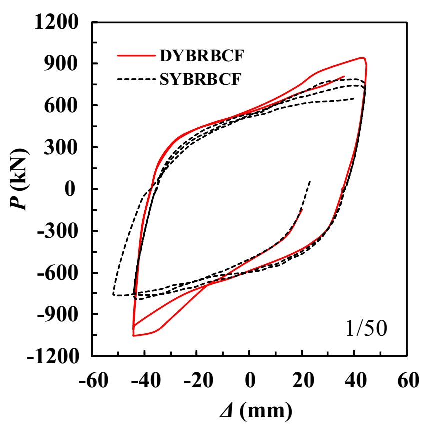

(i) Story drift ratio of 1/50

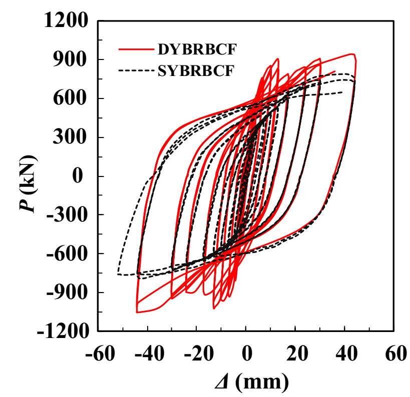

(j) Complete hysteretic curve of two specimens

Table 2 The horizontal force for the corresponding drift ratio (unit: kN)

Story drift ratio	SYBRBCF			DYBRBCF		
	+	–	Mean	+	–	Mean
1/2800	–	–	–	150.9	217.2	184.1
1/2000	–	–	–	197.7	284.1	240.9
1/1400	–	–	–	270.9	405.0	338.0
1/900	251.9	304.0	278.0	396.9	558.4	477.7
1/700	–	–	–	487.9	670.4	579.4
1/500	369.3	435.8	402.6	623.7	798.5	711.1
1/320	409.1	510.0	459.6	760.6	938.2	849.4
1/220	476.6	555.8	516.2	852.8	957.1	905.0
1/170	519.2	580.9	550.1	905.5	1024.5	965.0
1/130	563.8	655.8	609.8	789.7	894.3	842.0
1/95	691.0	695.3	693.2	851.9	897.5	874.7
1/75	750.2	729.8	740.0	908.5	946.6	927.6
1/50	764.1	756.4	760.3	939.6	1054.0	996.8

+, positive loading; –, negative loading

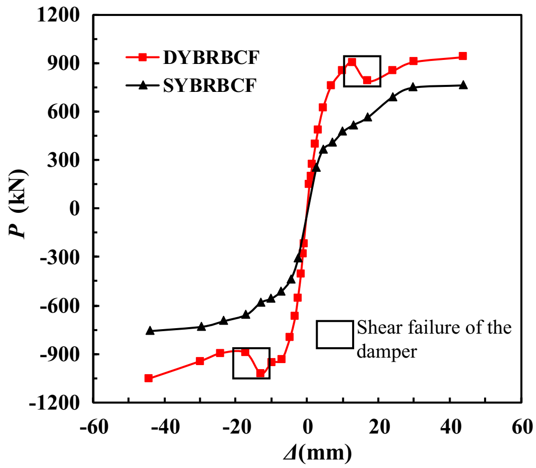

Fig. 15 Skeleton curve of the test specimens

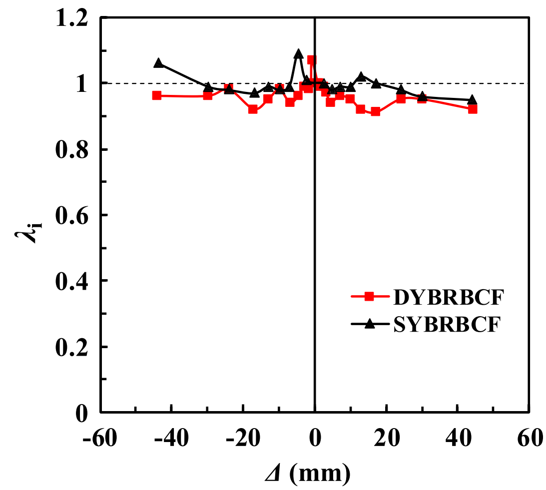

Fig. 16 Strength degradation curve of the test specimens

defined by Eqs. (13) and (14) [26], respectively, to evaluate the energy dissipation capacity.

$$E = \frac{S_{(ABC)} + S_{(CDA)}}{S_{(OBE)} + S_{(OBF)}}, \tag{13}$$

$$\xi_e = \frac{1}{2\pi}E, \tag{14}$$

where $S_{(ABC)}$, $S_{(CDA)}$, $S_{(OBE)}$, and $S_{(OBF)}$ are the areas surrounded by the corresponding points, as shown in Fig. 18.

Table 4 lists the energy consumption performance indicators of the specimens. The energy dissipation and equivalent damping ratios of the SYBRBCF increased gradually with an increase in the lateral displacement. By contrast, the energy dissipation and equivalent damping ratios of the DYBRBB initially decreased and then increased. The initial decrease in the DYBRBCF was due to the excessive initial stiffness. After the damper was destroyed, the energy dissipation and equivalent damping ratios of the SYBRBCF were higher than those of the DYBRBCF owing to the higher load-bearing capacity of the DYBRBCF. Figure 19 compares the total energy dissipation of the two specimens to better understand the energy dissipation capacity directly. As excepted, the DYBRBCF dissipated more energy during

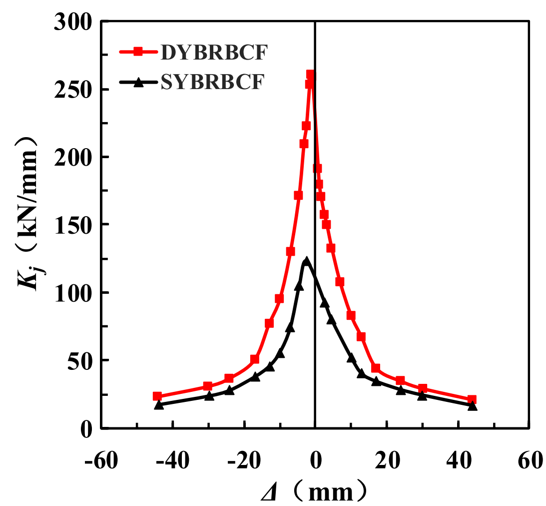

Fig. 17 Stiffness curve of the test specimens

Table 3 Primary performance indicators of the specimens

Specimen no.	Direction	K_0 (kN/mm)	P_y (kN)	D_y (mm)	θ_y	P_m (kN)	D_m (mm)	θ_m	D_u (mm)	θ_u	μ
SYBRBCF	+	93	510	12.3	1/184	752.0	43.6	1/50	43.6	1/50	3.5
	−	124	548	9.20	1/246	735.0	43.6	1/50	43.6	1/50	4.7
	Mean	108	529	10.8	1/211	744.0	43.4	1/50	43.4	1/50	4.1
DYBRBCF	+	191	780	6.00	1/377	980.0	44.0	1/50	44.0	1/50	7.3
	−	259	900	6.50	1/348	1150	45.0	1/50	45.0	1/50	6.9
	Mean	225	840	6.30	1/362	1065	44.5	1/50	44.5	1/50	7.1

K_0, initial stiffness; P_y, yield load; D_y, yield displacement; θ_y, yield story drift ratio; P_m, peak load; D_m, displacement of the peak load; θ_m, story drift ratio of the peak load; D_u, displacement of the ultimate load; θ_u, story drift ratio of the ultimate load; μ, ductility coefficient

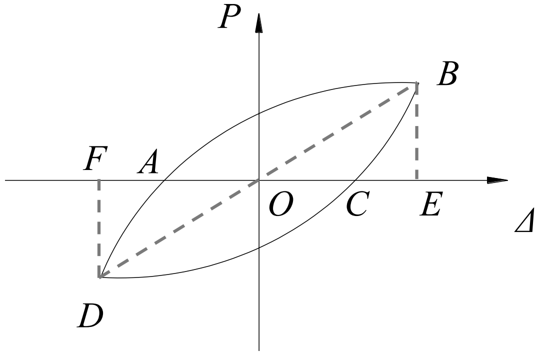

Fig. 18 Schematic of hysteresis loop

the cyclic load than the SYBRBCF, indicating that the DYBRBCF has a better energy dissipation capacity. The total energy dissipation of the DYBRBCF was 23.4% higher than that of the SYBRBCF. This condition might be caused by the additional damping of the DYBRBs during frequent earthquake events.

6 Conclusions

This paper presented a study on the seismic behavior of two types of buckling-restrained braced concrete frames. The working mechanism of double-level yielding buckling-restrained brace was introduced firstly. A SYBRBCF and a DYBRBCF were designed and subjected to cyclic loading. The seismic performance of SYBRBCF and DYBRBCF was evaluated and compared in detail. The main conclusions can be summarized as follows:

(1) The loading–displacement hysteretic curves of SYBRBCF and DYBRBCF were plump, indicating a favorable seismic behavior. No evident degradation of the load-bearing capacity occurred during the loading program, and the degradation of the stiffness was stable. The strength degradation was slight, indicating the stable load-bearing capacity of the specimens.

(2) The concrete frame can coordinate with the SYBRB and DYBRB under earthquake. The failure modes of the two specimens were similar and satisfied the strong-column–weak-beam design concept. However, the DYBRB can better reduce the seismic damage of the concrete frame than the SYBRBCF.

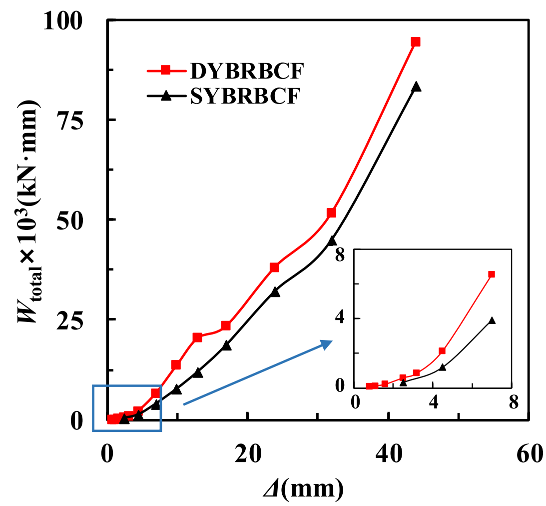

Fig. 19 Energy dissipation curve of the test specimens

Table 4 Energy consumption performance indicators of the specimen

Story drift ratio	SYBRBCF			DYBRBCF			SYBRBCF/DYBRBCF		
	$W_{total,s}\times10^3$ (kN mm)	E_s	$\xi_{e,s}$	$W_{total,d}\times10^3$ (kN mm)	E_d	$\xi_{e,d}$	$W_{total,s}/W_{total,d}$	E_s/E_d	$\xi_{e,s}/\xi_{e,d}$
1/2800	–	–	–	0.080	0.54	0.09	–	–	–
1/2000	–	–	–	0.120	0.44	0.07	–	–	–
1/1400	–	–	–	0.210	0.40	0.06	–	–	–
1/900	0.33	0.47	0.08	0.600	0.49	0.08	0.57	0.97	0.97
1/700	–	–	–	0.850	0.46	0.07	–	–	–
1/500	1.20	0.65	0.10	2.140	0.70	0.11	0.56	0.92	0.92
1/320	3.91	1.17	0.19	6.540	1.16	0.19	0.60	1.00	1.00
1/220	7.71	1.47	0.23	13.62	1.57	0.25	0.57	0.93	0.93
1/170	12.0	1.64	0.26	20.37	1.73	0.28	0.59	0.95	0.95
1/130	18.6	1.78	0.28	23.36	1.82	0.29	0.80	0.97	0.97
1/95	32.2	1.99	0.32	38.17	1.88	0.30	0.84	1.06	1.06
1/75	45.0	2.10	0.33	51.72	1.93	0.31	0.87	1.08	1.08
1/50	83.5	2.52	0.40	94.59	2.16	0.34	0.88	1.17	1.17

(3) The DYBRB can provide additional damping for structures under frequent earthquake events and an excellent energy dissipation capacity under rare earthquake events as based on the test results.
(4) The DYBRBCF achieves a higher load-bearing capacity and stiffness. The maximum values of the lateral load and initial stiffness were enhanced by 39.3% and 109.8%, respectively. The test results imply that the design concept of the DYBRB is reasonable.
(5) The loading–displacement hysteretic curves of the DYBRBCF were fuller than those of the SYBRBCF. The DYBRBCF also exhibited a better ductility and energy dissipation capacity than those of the SYBRBCF. The ductility coefficient and total energy dissipation were enhanced by 72.2% and 23.4%, respectively. Therefore, DYBRBs can further improve the seismic performance of the concrete frame.

Acknowledgements The research reported in this paper was funded by the National Natural Science Foundation of China (No. 51908511), China Postdoctoral Science Foundation (No. 2019M662532), Key Scientific Research Projects of Henan Higher Education Institutions (No. 20A560001), Postdoctoral Research Grant in Henan Province (No. 1902022), and Outstanding Young Talent Research Fund of Zhengzhou University (No. 1421322062).

Compliance with ethical standards

Conflict of interest We wish to confirm that there are no known conflicts of interest associated with this publication and there has been no significant financial support for this work that could have influenced its outcome.

Ethical statement Ethics Committee approval was obtained from the Institutional Ethics Committee of Zhengzhou University to the commencement of the study.

References

1. Ranaei O, Aghakouchak AA. A new hybrid energy dissipation system with viscoelastic and flexural yielding strips dampers for multi-level vibration control. Arch Civ Mech Eng. 2019;19(2):584–97.
2. Massumi A, Absalan M. Interaction between bracing system and moment resisting frame in braced RC frames. Arch Civ Mech Eng. 2013;13(2):260–8.
3. Khampanit A, Leelataviwat S, Kochanin J, Warnitchai P. Energy-based seismic strengthening design of non-ductile reinforced concrete frames using buckling-restrained braces. Eng Struct. 2014;81:110–22.
4. Wu H, Zhang GW, Zhao J, Zhang Y. Seismic performance of existing RC frame structures reinforced with buckling-restrained braces. Civ Eng J. 2013;46(7):37–45 **(in Chinese)**.
5. Fujimoto M, Wada A, Saeki E, Watanabe A, Hitomi Y. A study on brace enclosed in buckling-restraining mortar and steel tube. In: Summaries of technical papers of AIJ annual meetings (1988). p. 1339–1342 (in Japanese).
6. Fujimoto M, Wada A, Saeki E, Takeuchi T, Watanabe A. Development of unbonded brace. Q Column. 1990;115:91–6.
7. Bozkurt MB, Topkaya C. Development of welded overlap core steel encased buckling-restrained braces. J Constr Steel Res. 2016;127:151–64.
8. Zhu BL, Guo YL, Zhou P, Bradford MA, Pi YL. Numerical and experimental studies of corrugated-web-connected buckling-restrained braces. Eng Struct. 2017;134:107–24.
9. Qu B, Liu X, Hou H, Qiu C, Hu D. Testing of buckling restrained braces with replaceable energy dissipating angle fuses. J Struct Eng. 2018;3(144):04018001-1–04018001-14.
10. Guo YL, Zhang BH, Jiang ZQ, Zhao SY. Elastic buckling analysis of core-separated buckling-restrained braces by Ritz method. Eng Mech. 2015;32:26–35 **(in Chinese)**.
11. Guo YL, Zhang BH, Jiang ZQ, Chen H. Critical load and application of core-separated buckling-restrained braces. J Constr Steel Res. 2015;106:1–10.
12. Guo YL, Zhang BH, Zhu BL, Zhou P, Zhang YH, Tong JZ. Theoretical and experimental studies of battened buckling-restrained braces. Eng Struct. 2017;136:312–28.
13. Wang JF, Li BB, Chou CC, Chen L. Cyclic experimental and analytical studies of buckling-restrained braces with various gusset connections. Eng Struct. 2018;163:38–52.
14. Tsai KC, Lin PC, Wu AC, Chuang MC, Li CH, Wang KJ. Seismic design and experiment of single and coupled corner gusset connections in a full-scale two-story buckling-restrained braced frame. Earthq Eng Struct Dyn. 2015;44(13):2177–98.
15. Zhang GW, Chen P, Zhao ZW, Wu JF. Experimental study on seismic performance of rocking buckling-restrained brace steel frame with liftable column base. J Constr Steel Res. 2018;143:291–306.
16. Qu Z, Xie JZ, Wang T, Kishiki S. Cyclic loading test of double K-braced reinforced concrete frame subassemblies with buckling restrained braces. Eng Struct. 2017;139:1–14.
17. Boostani M, Rezaifar O, Gholhaki M. Introduction and seismic performance investigation of the proposed lateral bracing system called “OGrid”. Arch Civ Mech Eng. 2018;18(4):1024–41.
18. Chou CC, Chen SY. Subassemblage tests and finite element analyses of sandwiched buckling-restrained braces. Eng Struct. 2010;32(8):2108–21.
19. Chen LW, Tsai KC, Tsai CY, Wu AC. Evaluating out-of-plane stability for welded BRBs considering flexural restrainer and gusset rotations. J Constr Steel Res. 2019;159:161–75.
20. AlHamaydeh M, Abed F, Mustapha A. Key parameters influencing performance and failure modes for BRBs using nonlinear FEA. J Constr Steel Res. 2016;116:1–18.
21. Li GQ, Sun YZ, Jiang J, Sun FF, Ji C. Experimental study on two-level yielding buckling-restrained braces. J Constr Steel Res. 2019;159:260–9.
22. Sun YZ, Li GQ, Sun FF. Parametric analysis of frames with two-level-yielding buckling restrained braces under frequent earthquake. J Arch Civ Eng. 2019;36(6):88–94 **(in Chinese)**.
23. GB 50011-2010(2016). Code for seismic design of buildings, Beijing. 2016 (in Chinese).
24. GB 50010-2010(2015). Code for design of concrete structures, Beijing. 2015 (in Chinese).
25. Cheng GY, Ye LP, Cui HC. Study on the design method of buckling-restrained brace. J Build Struct. 2008;29(1):40–8 **(in Chinese)**.
26. Li ZX. Theory and technique of engineering structure experiments. Tianjin: Tianjin University Press; 2004 **(in Chinese)**.